Native point defects and doping in $ZnGeN_2$

Dmitry Skachkov, Atchara Punya Jaroenjittichai,* Ling-yi Huang, and Walter R. L. Lambrecht
Department of Physics, Case Western Reserve University, Cleveland, Ohio 44106-7079, USA
(Received 30 November 2015; revised manuscript received 11 March 2016; published 11 April 2016)

A computational study within the framework of density functional theory in the local density approximation (LDA) is presented for native defects and doping in $ZnGeN_2$. Gap corrections are taken into account using an LDA+U approach and finite size corrections for charged defects are evaluated in terms of an effective charge model, introduced in this paper. The donor or acceptor characteristics of each of the cation and N vacancies and the two cation antisite defects are determined as well as their energies of formation under different chemical potential conditions. These are then used to determine defect concentrations and Fermi level pinning self-consistently. The cation antisite defects are found to have significantly lower formation energy than the cation vacancies. At a typical growth temperature of 1200 K, the charge neutrality condition pins the Fermi level close to the crossing of the formation energies of the Zn_{Ge}^{-1} acceptor with the Ge_{Zn}^{2+} shallow donor. Since this point lies closer to the valence-band maximum (VBM), intrinsic p-type doping would result at the growth temperature and will persist at room temperature if the defect concentrations are frozen in. It is the highest and of order 10^{16} cm^{-3} for the most Ge-poor condition. On the other hand, for the most Ge-poor condition, it drops to 10^{13} cm^{-3} at 1200 K and to almost zero at 300 K because then the Fermi level is too close to the middle of the gap. Oxygen impurities are found to strongly prefer the O_N substitutional site and are found to be shallow donors with a very low energy of formation. It can only be suppressed by strongly reducing the oxygen partial pressure relative to that of nitrogen. At high temperatures, however, introduction of oxygen will be accompanied by compensating Zn_{Ge}^{-2} acceptors and would lead to negligible net doping. The prospects for Ga base p-type doping are evaluated. While good solubility is expected, site competition between Zn and Ge sites is found to lead to a compensation problem similar to that of the two antisites and leads to p-type doping of the same level of 10^{16} cm^{-3}.

DOI: 10.1103/PhysRevB.93.155202

I. INTRODUCTION

$ZnGeN_2$ is a heterovalent semiconductor, related to wurtzite GaN, from which it can conceptually be derived by replacing Ga (which is a group-III element) by equal amounts of Zn (group II) and Ge (group IV). If this is done in such a fashion that each N is surrounded by exactly two Zn and two Ge, then the octet rule of bonding is locally satisfied and leads to a band structure and other properties with great similarity to GaN. It is thus a potential replacement for GaN or at least an addition to the family of group-III nitrides in various technological applications, notably light-emitting diodes, lasers, ultraviolet light sensors, and other optoelectronic devices, as well as high-electron-mobility transistors, that all rely on the wide and direct band gap of this material. In a broader context, moving from binary and pseudobinary isovalent semiconductors to the class of heterovalent ternary semiconductors could offer new avenues for band-structure and defect engineering. $ZnGeN_2$ is part of a broader family of II-IV-N_2 semiconductors and the best studied member of the family. Nonetheless, very little is currently known about its defect physics.

Band structures of the Zn-IV-N_2 compounds with IV = Si, Ge, Sn were studied previously in our group, using the quasiparticle self-consistent QSGW method [1]. Lattice dynamical properties of this family of materials were studied in Refs. [2–4]. For an overview of the properties of these materials, their growth methods, including work by other research groups, we refer the reader to a review in Ref. [5]. The general motivation for the study of this materials family is that heterovalent ternaries may enrich the physics of the usual binary semiconductors. By their lower symmetry, they offer new opportunities for optical applications. Combining them with the family of III-nitrides, new flexibilities are added in device design.

The observed ordering of the Zn and Ge atoms corresponds to a $Pna2_1$ space group with orthorhombic symmetry and a 16 atom unit cell. The role of the octet rule and possible origins of disorder in $ZnGeN_2$ were recently studied by Quayle *et al.* [6]. One of the central questions in this family of materials is indeed to what extent the group-II and group-IV atoms are ordered or disordered. Both ordered and disordered phases have been observed experimentally depending on growth conditions. In Quayle *et al.* [6] it is proposed that the observed disordered phase properties, such as the Raman spectra, x-ray diffraction (XRD) spectra and photoluminescence or band gap insensitivity to disorder could be explained in terms of a model which strictly observes the octet rule locally. In other words, instead of a fully random distribution of Zn and Ge over the cation sublattice, a more restricted distribution was postulated which preserves locally that each N is surrounded by exactly two Zn and two Ge atoms. In other works [7], more precisely on $ZnSnN_2$, it was proposed that disorder could strongly affect the band gap. In the above work by Quayle *et al.* [6] it was argued that this might primarily be due to exchange defects which break the octet rule. As a preliminary to the studying such exchange defects, which amount to complexes of Zn_{Ge} (Zn on a Ge site) with Ge_{Zn} antisites, a thorough understanding of simple point defects seems in order.

The defect physics in a heterovalent semiconductor such as $ZnGeN_2$ is far more complex than in a binary compound. For

*Present address: Department of Physics and Materials Science, Chiang Mai University, 239 Huay Kaew Road, Muang, Chiang Mai 50200, Thailand.

example, there is now the possibility of cation antisite disorder, Zn_{Ge} and Ge_{Zn} as well as two types of cation vacancies, V_{Zn} and V_{Ge}. Important questions are, which of these defects are more likely to occur and how do they influence the position of the Fermi level? One might expect that deviations from perfect stoichiometry could dope the material since Zn_{Ge} is expected to be an acceptor and Ge_{Zn} to be a donor. In previous preliminary considerations about the defect physics, for example, in Ref. [5], we noted that if one would like to dope the material p type by introducing Ga on Ge sites rather than Ga on Zn sites, one would work in Ge-poor conditions. At the same time this would promote Zn_{Ge} antisites, which are also expected to be acceptors. This contrasts with the usual notion that in wide-band-gap semiconductors, introducing acceptor dopants would promote compensating native donors. Other sources of undesirable n-type background doping in GaN, for example from Si impurities resulting from the quartz tubes used in metalorganic chemical vapor deposition (MOCVD), would not be expected to be dopants in $ZnGeN_2$ because Si is isovalent with Ge. Thus it seems that the heterovalent nitrides may have advantages over binary nitrides for p-type doping. This is important because high levels of p-type doping are still a limiting factor in nitride devices. The technological achievement of high efficiency blue LEDs was based in large part on the breakthrough of achieving p-type doping. So, p-type doping is a central goal in nitride technology.

Although there thus may possibly be advantages for II-IV-N_2 materials in terms of doping, confirmation of this proposal requires a thorough investigation of its point defect physics. As we will show in this paper, the above mentioned ideas of about Ga doping and doping by stoichiometry variation depend crucially on their energies of formation and the resulting Fermi-level pinning in the gap. Secondly, when considering doping by group-III elements such as Ga, we need to evaluate the effects of the site competition since Ga on the Zn site would be a donor and Ga on the Ge site would be an acceptor. Finally, the effects of commonly observed impurities such as oxygen need to be evaluated.

In this paper we present a comprehensive study of native defects, including V_{Ge}, V_{Zn}, V_N, Zn_{Ge}, and Ge_{Zn}. We also considered O_N, a commonly found impurity and possibly n-type dopant, as well as Ga_{Zn} and Ga_{Ge} prospective dopants. First, however, we present our computational method in some detail, in particular the aspects which related to supercell size effects.

II. COMPUTATIONAL METHODS

A. General aspects

Our calculations are based on density functional theory [8,9] in the local density approximation (LDA) [10]. We use the full-potential linearized muffin-tin orbital method as implemented in the lm suite [11] and described in Methfessel *et al.* [12] and Kotani *et al.* [13]. To test the effects of the gap underestimate by LDA, we also used the LDA+U approach, which allows us to open the gap as explained below. Specific aspects of this method relating to defect calculations are as follows.

We used a $2 \times 2 \times 2$ supercell of the 16 atom primitive cell of $ZnGeN_2$, which thus contains 128 atoms. The atomic positions were fully relaxed. To accelerate this process, we found it useful to use a finite temperature smearing around the Fermi level, which allows us to keep the **k**-point mesh minimal. Tests were done for either a single **k** point or a symmetrized $2 \times 2 \times 2$ mesh and the final results for the energies of formation were calculated with the larger mesh.

B. Charged defects

Charged defect states were compensated by a uniform background charge density. This uniform background is required to obtain meaningful electrostatic energies. One may also interpret it as representing the screening charge density. In the FP-LMTO code, it is fully taken into account, not just to fix the reference level in the Madelung potential. For example, inside the spheres, a uniform charge density does not produce a constant potential. While we have used this form of implementing the background charge density since we started work on point defects [14], it differs from usual practice. The importance of this was recently pointed out by Bruneval *et al.* [15].

Subsequently, we calculate the band structures and the local densities of states on the atoms neighboring the defect site so as to inspect their basic electronic properties. The defect wave functions $\psi_D(\mathbf{r})$ or rather $|\psi_D(\mathbf{r})|^2$ were calculated by integrating over a small energy window bracketing the defect band and visualized as a constant value surface for several states of interest. This is used to determine whether or not certain states were localized or more delocalized.

C. Energies of formation

We calculate the energies of formation using the equation

$$E_{\text{for}}(D,q) = E_{\text{tot}}(D,q) - E_{\text{tot}}(X) + \sum_i \mu_i \Delta n_i + q(\epsilon_v + \epsilon_F + V_{\text{align}}) + E_{\text{corr}}. \quad (1)$$

Here, $E_{\text{for}}(D,q)$ is the energy of formation of defect D in charge state q, $E_{\text{tot}}(D,q)$ is the corresponding total energy of the supercell, from which we actually already subtracted the free atom energies, $E_{\text{tot}}(X)$ is the supercell total energy of the perfect crystal calculated in the same size supercell. The chemical potentials μ_i depend on the reservoirs to which atoms for a defect are removed or from which additional atoms are taken and depend on the growth conditions. The Δn_i represent the changes in occupation of the various atomic species in the defect system relative to the perfect crystal. For example, for a Zn_{Ge}, $\Delta n_{Ge} = +1$ and $\Delta n_{Zn} = -1$.

D. Chemical potentials of the atoms

The allowed ranges of the chemical potentials are determined by equilibrium with the host material, and various other binary compounds, i.e., Zn_3N_2 and Ge_3N_4, bulk Ge, bulk Zn, and N_2 molecules (see Fig. 1):

$$\begin{aligned} \mu_{Ge} + \mu_{Zn} + 2\mu_N &= \mu_{ZnGeN_2}, \\ 3\mu_{Zn} + 2\mu_N &\leqslant \mu_{Zn_3N_2}, \\ 3\mu_{Ge} + 4\mu_N &\leqslant \mu_{Ge_3N_4}, \\ \mu_{Ge} \leqslant 0, \mu_{Zn} &\leqslant 0, \mu_N \leqslant 0. \end{aligned} \quad (2)$$

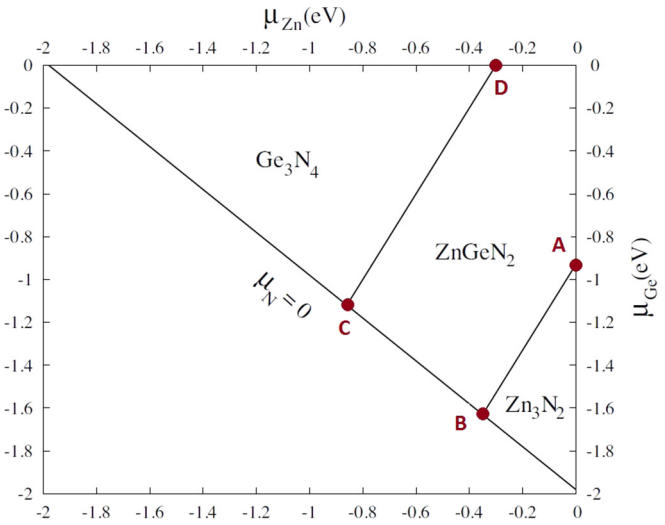

FIG. 1. Chemical potential diagram for $ZnGeN_2$.

Here the chemical potential are defined relative to their reference values for each element in its state naturally occurring at room temperature and standard pressure. In other words, $\mu_i = \mu_i^{\text{abs}} - \mu_i^0$. The reference values μ_{Ge}^0 correspond to bulk Ge in the diamond structure, μ_{Zn}^0 to bulk metallic Zn and μ_{N}^0 to the N_2 molecule. The total energies in Eq. (1) are then similarly defined by already subtracting the reference state chemical potentials. The values used here are slightly changed from previous work [5] to reflect our updated calculations of the energy of formation of $ZnGeN_2$ [6]. The first equation in Eq. (2) is an equality because we assume definitely equilibrium with the host material. Thus one of the three chemical potentials is fixed in terms of the other two by the equilibrium condition with $ZnGeN_2$. We choose μ_{Ge} and μ_{Zn} as independent variables. The diagonal line (BC) $\mu_{\text{Ge}} + \mu_{\text{Zn}} = E_{\text{for}}(ZnGeN_2)$ corresponds to the N-rich condition $\mu_{\text{N}}^{\text{abs}} = \mu_{\text{N}}^0$ or $\mu_{\text{N}} = 0$. The region where $ZnGeN_2$ is stable is delimited by the labels A-D and the origin. When adding impurities, such as Ga and O, we also need to fix their chemical potentials. As usual, this is done by assuming they have the chemical potential of their standard reference states, bulk metallic Ga or an O_2 molecule. However, if the system is N-rich, we may also assume that Ga is in equilibrium with GaN. For O, we will study the behavior as function of the partial pressure of O_2 relative to that of N_2.

E. Alignment potential

The last two terms in Eq. (1) represents the chemical potential of the electrons and the periodic image potential correction. The Fermi level with respect to the valence-band maximum (VBM) is ϵ_F and the VBM one-electron energy is ϵ_v. The latter needs to be calculated with respect to the cell-averaged electrostatic potential. Because the average electrostatic potential in a periodic system is not a well-defined quantity, an alignment shift is required between the potential at an atom far away from the defect in the supercell containing defect and the corresponding potential in the perfect crystal. For a neutral system, this is easily determined because it quickly converges but for a charged system, it varies slowly

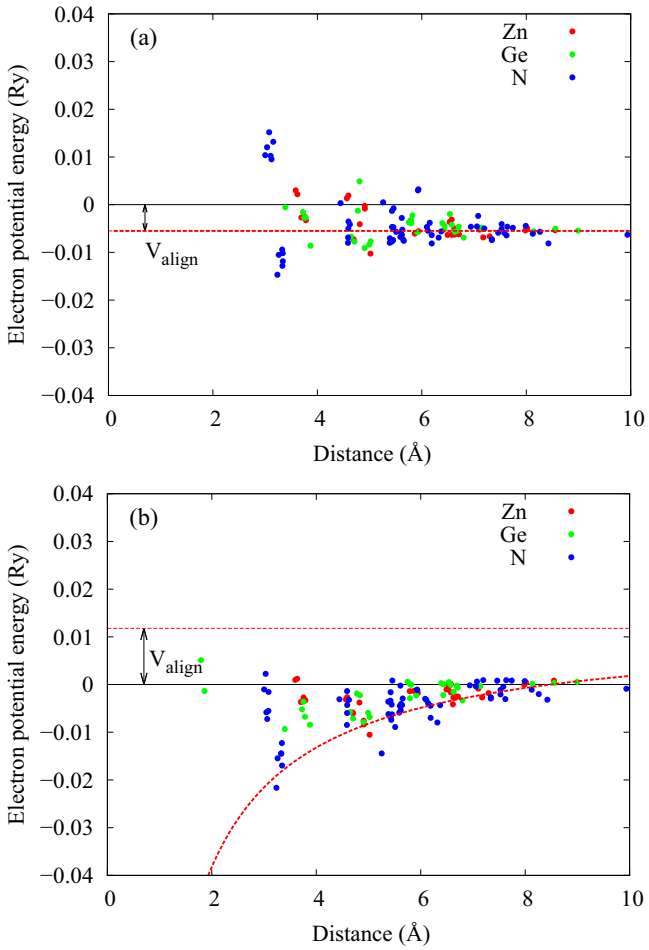

FIG. 2. Electrostatic potential energy of an electron for the V_{N} defect for the $q = 0$ (a) and $q = +1$ (b) charge states with respect to the potential in the perfect crystal as a function of distance from the defect. The differently colored symbols correspond to potentials on different sites. For the $q = 1$ state, the red dashed curve represents the point charge potential $q/\varepsilon d$ and the horizontal red dashed line is its asymptote, which gives the alignment potential.

as $q/\varepsilon d$ with d the distance from the defect. We followed the recommendations of a recent paper by Kumagai *et al.* [16] in this respect of analyzing and visualizing this dependence in the full 3D space. This procedure is essentially equivalent to that proposed by Freysoldt *et al.* [17–19], although it differs in some practical aspects. For example, Freysoldt *et al.* typically use a continuous 2D averaged form of the defect model charge potential to determine the alignment whereas we use a discretized radial distribution. We do not here include the anisotropic treatment of the point charge background interaction introduced by Kumagai *et al.* [16] because the material under study is not expected to exhibit low-dimensional or strongly anisotropic aspects.

Our procedure is illustrated in Fig. 2 for the case of the nitrogen vacancy in the neutral and +1 charge states. First, we determine electrostatic potential values at the muffin-tin radii of all atoms in the supercell relative to those of the corresponding atom in the host unit cell. These are shown as differently colored circles for the different types of atoms.

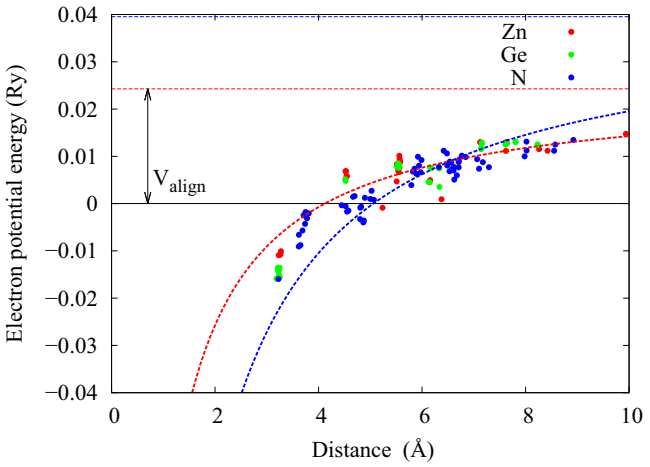

FIG. 3. Electrostatic potential energy of an electron for the Ge_{Zn} defect for the $q = +2$ charge state. The blue dashed line corresponds to $q = +2$, and the red dashed line corresponds to $q_{\text{eff}} = +1$.

Note that we plot the electrostatic energy of an electron, so it is lower near a positively charged defect. We plot them as function of distance to the defect site to which they are nearest in the periodic structure. In case of a neutral defect, we can then easily determine the average over the region where this alignment potential difference becomes flat, i.e., beyond a minimum distance from the defect center, about 4.5 Å in practice. For a charged defect with a well-localized defect net defect charge, however, there is still a systematic variation to this potential, which is well described by $V_{\text{align}} + q/\varepsilon d$. Here, ε is the static dielectric constant, for which we use a value of $\sim$10 and we use atomic units. After we subtract $q/\varepsilon d$, a region where the average of these potentials looks flat can again be obtained beyond some distance. So, V_{align} is determined by averaging over this region after subtracting $q/\varepsilon d$. This $V_{\text{align}} = \Delta V_{0/b} + \Delta V_{q/0} = \Delta V_{q/b}$ in Freysoldt *et al.* 's notation [17] includes both $\Delta V_{0/b}$, which is the difference in average potential between the neutral defect and bulk host system which simply arises from the arbitrariness of the average potential, and $\Delta V_{q/0}$, which the change between the charged and neutral average potentials which results from the periodic arrangement of the net point charges in the neutralizing background. In some cases, notably for shallow donor states, we find that potential is better described by an effective rather than the nominal charge of the defect. A related concept was earlier introduced by Oba *et al.* [20] by using a net charge even for neutral shallow defects. It is illustrated here for the case of Ge_{Zn}^{2+}. While the nominal charge of the defect is $+2$, it is clearly seen in Fig. 3 that the potential near the defect is better described using $q_{\text{eff}} = +1$. A way to think about this is that part of the defect electronic charge is delocalized and simply reduces the corresponding background, while part stays localized near the defect because of the nuclear charge. This model is thus similar to the model charge distribution consisting of a localized Gaussian of reduced charge plus a fully delocalized remainder of the charge as used by Komsa *et al.* [21] for delocalized cases, such as V_C^{+2}. For the region far away from the defect, the potential produced by a localized Gaussian or a point charge should be the same since the potential outside a spherical charge distribution only depends on its net charge. The important point is that the net charge is reduced because of the delocalization.

F. Image potential corrections

Consistent with this point charge model potential, we then need to add a point charge correction to the total energy for the charged defect system. This term represents the Madelung energy of the point charges embedded in the back ground charge density. However, when the net charge of the defect is q_{eff} this becomes $E_{\text{Mad}} = -\alpha q_{\text{eff}}^2/(2\varepsilon L)$, which converges slowly as $1/L$, with L the size of the system. This correction term was first considered by Leslie and Gillan [22]. In practice, we calculate the Madelung constant assuming a spherical model of the supercell, which gives $\alpha/(2L) = 9/(10R_{WS})$ with $4\pi R_{WS}^3/3 = V_{\text{cell}}$. We here use the static dielectric constant, consistent with the fact that all atomic positions are relaxed and thus atomic displacements contribute to the screening. In other words, a correction energy $E_{\text{corr}} = -E_{\text{Mad}}$ is added thereby extrapolating to the $L \to \infty$ limit. Note that both this term and the alignment term are calculated with q_{eff}, but the terms $q(\epsilon_v + \epsilon_F)$ maintain the nominal charge.

This model works well as long as the defect charge density is sufficiently well localized within the supercell. For a shallow defect this is not the case. In fact, while in reality there will then be an effective-mass-like or hydrogenic defect level slightly (of order a few tens of meV) below the conduction band (for a donor) or slightly above the VBM (for an acceptor), in the calculations, we find no states in the gap at all, and instead a filling of the bottom of the conduction band (or depletion of the top of the valence band). This situation occurs here, for example, for Ge_{Zn}. In this case, the charge density for the charged or neutral state of the donor is similar because in the charged state, we add a background charge density, while in the neutral charge state, the electrons are spread out nearly uniformly in the conduction band. This is why for the Ge_{Zn} case we find that the potential around the defect looks rather similar in the 0, $+1$, and $+2$ states. Segev and Wei [23] noted that if the defect charge density is modeled as a Gaussian distribution rather than a point charge, the correction decreases to zero when the width of a Gaussian defect model distribution is increased. However, although the electronic contribution to the defect charge density is spread out, the net charge density including electron plus nuclear charge is still quite localized (because of the nuclear charge discrepancy between defect and host) and a point charge correction is still needed for the $2+$ charge state. In this case, we calculate it with q_{eff}. On the other hand, for the neutral charge state, or $+1$ we can then determine the energy of formation from the consideration that the transition state $2+/+$ should occur essentially at the shallow level just below the conduction-band minimum (CBM). This approach is similar to the one proposed by Kumagai *et al.* [24]. In agreement with their conclusion, we find that this is equivalent to adding a point charge correction even for the neutral charge state.

As was discussed, for example, by Komsa *et al.* [21] and Freysoldt *et al.* [18,19], there is then no need any more for the quadrupole correction term introduced by Makov and

Payne [25] because the latter is equivalent to the alignment term and both vary as $1/L^3$ with the size of the supercell.

G. LDA+U gap corrections

The local density approximation (LDA) is known to severely underestimate band gaps and this may affect defect levels. For a shallow donor or acceptor, it is pretty clear that the defect states will just follow the conduction or valence band, respectively, when gap corrections are applied. However, for a deep level, it is less clear. Therefore we need an explicit way to correct the gap. Ideally, we would use GW calculations if we study the one-electron levels. However, the GW method is still very time consuming for large systems. An alternative is provided by the LSDA+U method [26–29]. In its simplest form [29], in the LSDA+U method, an atomic orbital (or more generally a localized basis set orbital or partial wave inside a muffin-tin sphere) i is shifted by

$$V_i = U_i\left(\frac{1}{2} - n_i\right), \tag{3}$$

where n_i is the occupation number of that orbital. In other words, if the orbital is completely occupied ($n_i = 1$) its orbital energy is shifted by $-U_i/2$ and if the orbital is empty ($n_i = 0$), its orbital energy is shifted up by $U_i/2$. While this method was originally introduced to deal with partially filled shells of localized orbitals, such as d or f states in transition metals or rare earths, we here apply it to the orbitals that primarily determine the gap-edge states. This approach was used successfully previously for defects in ZnO [30,31]. The valence-band maximum is N-p like. However, we found in previous QSGW calculations [1] of $ZnGeN_2$ that the VBM essentially does not shift. The gap correction is completely carried by the CBM. Therefore we instead look at the orbital composition of the CBM. It is formed primarily from Ge-s, Ge-p, Zn-s, and Zn-p states. The CBM at Γ is more predominantly formed by the s-states but the states in the rest of the BZ have also strong p contributions. We found that we obtain an almost rigid shift gap correction throughout the Brillouin zone by applying both s and p U shifts on both Zn and Ge. Specifically with $U_{\mathrm{Ge}-s} = 3.5$ Ryd, $U_{\mathrm{Zn}-s} = 3.5$ Ryd, $U_{\mathrm{Ge}-p} = 2.4$ Ryd, $U_{\mathrm{Zn}-p} = 2.4$ Ryd, we obtain a direct gap of 3.4 eV and a more or less rigid shift of the conduction band at other **k** points. In other words, this LSDA+U model provides good agreement with the QSGW results of Ref. [1], which was there shown to agree well with experiment. This may not be a unique solution but it provides a good model to examine what the effect of the conduction-band shift is on defect levels.

We caution that it is not *a priori* clear that an LSDA+U model would capture the gap correction and even if it does so, it is not clear it does so for the right reasons. We know that the actual GW self-energy Σ is a nonlocal operator and in fact probably fairly long range. So, it is not evident at all that its effect can be mimicked correctly by a local shift of certain atomic orbitals. The values we need for U_i may also seem extremely large or unphysical. This is in part because the occupation numbers are not really zero or one. In the bonding, charge is transferred from Zn and Ge to N, so one expects the occupation numbers of the Zn and Ge dangling bonds to be less than 1/2 but they are not zero because the bonding states have some Zn and Ge character. Also, the conduction-band states are not purely the corresponding atomic orbital basis states. Thus the correction will be in the right direction but we need a fairly large U to shift reproduced the actual band gap. What is more important is that the potential shifts V_i in Eq. (3) are physically reasonable. We also do not claim or use the LSDA+U approach here for other properties of the material, only as a device to inspect the effect of gap shifts on the one-electron levels.

Nonetheless, the physics we capture with this model, is that if a defect wave function is conceptually decomposed into a conduction and valence-band-like state of the host, then the defect state will shift in proportion to how much it is valence or conduction band like and this is captured by applying shifts to the atomic orbitals that primarily define these states. In other words, defect states that are strongly N-like will not shift in our model but states that have a strong Zn or Ge s or p contribution will shift up. In other words, our model will be most useful to check the behavior of donor states. If the defects move up along with the conduction band, they can be considered shallow donors. However, if the correction shifts them less than the conduction band, it would make the donor level deeper. In some cases, it might also change defect resonances occurring above the CBM in LDA into actual defect levels in the gap.

TABLE I. Displacement (in Å) of nearest atoms with respect to the defect site.

Structure	Zn	Ge	N
V_{Ge}^{0}			0.16; 0.26; 0.22; 0.27
V_{Ge}^{-2}			0.19; 0.25; 0.22; 0.24
V_{Zn}^{0}			0.19; 0.20; 0.18; 0.14
V_{Zn}^{-2}			0.13; 0.18; 0.14; 0.13
V_{N}^{0}	0.16; 0.07	−0.08; −0.11	
V_{N}^{+1}	0.20; 0.12	−0.02; −0.08	
$\mathrm{Zn}_{\mathrm{Ge}}^{0}$			0.09; 0.11; 0.10; 0.11
$\mathrm{Zn}_{\mathrm{Ge}}^{-2}$			0.11; 0.13; 0.11; 0.12
$\mathrm{Ge}_{\mathrm{Zn}}^{+2}$			−0.12; −0.12; −0.13; −0.13
$\mathrm{O}_{\mathrm{N}}^{+1}$	0.12; 0.09	0.06; 0.06	
$\mathrm{Ga}_{\mathrm{Zn}}^{+1}$			−0.06; −0.07; −0.07; −0.07
$\mathrm{Ga}_{\mathrm{Ge}}^{0}$			0.05; 0.05; 0.05; 0.05
$\mathrm{Ga}_{\mathrm{Ge}}^{-1}$			0.05; 0.05; 0.05; 0.05

III. RESULTS

A. Relaxed structures

We start by discussing the relaxed structures of the defects. Table I shows the displacements of the nearest atoms to the defect from their idealized positions in the perfect crystal for

various charge states. Positive (negative) values mean outward (inward) displacements. Except for two cases (O_{Zn} and O_{Ge}) the displacement of the defect atom itself (Zn_{Ge}, Ge_{Zn}, O_N, Ga_{Ge}, and Ga_{Zn}) with respect to the idealized position is very small. For O_{Zn} and O_{Ge}, the displacement of the O atom from the missing Zn (Ge) atom position is 0.74 (0.43) Å. Displacements of similar magnitude occur for the charged states. The defects have no symmetry, since the site point group consists only of the identity. For the cation vacancies, the atoms move outward but slightly less for the negative charge state. For the Zn_{Ge} the relaxation is also outward, which is consistent with the larger Zn-N than Ge-N bond length. The outward relaxation of nearest N atoms becomes larger for negative charge states in contrast to the cation vacancies V_{Zn} and V_{Ge}. For Ge_{Zn}, an inward relaxation is observed, again consistent with the bond lengths. The inward relaxation slightly increases for the $q = +2$ state. Following the same trend, there is an inward relaxation near a Ga_{Zn} but an outward relaxation of Ga_{Ge}. Near the V_N^0, the Ge atoms move in and the Zn move out. In the $q = +1$ state, the defect V_N^{+1} pushes back both Zn and Ge atoms and inward relaxation of Ge atoms slightly decreases whereas outward relaxation of Zn slightly increases. For the O_N defect, both Zn and Ge atoms have outward relaxation.

B. Qualitative discussion of defect levels

In this section, we discuss the qualitative nature of the defects studied by examining their one-electron band structure, density of states, and defect wave functions.

1. Cation vacancies

We start with the V_{Ge} in the neutral charge state. Figure 4 shows the supercell band structure and partial densities of states (PDOS) on the nearest neighbor atoms. An empty sphere E is located on the vacancy site itself, so we can also examine the partial wave projected density of states on the defect site. We can see that a sharp peak occurs in the PDOS just above the VBM corresponding to three localized bands, which are partially occupied. This can be understood as follows. In

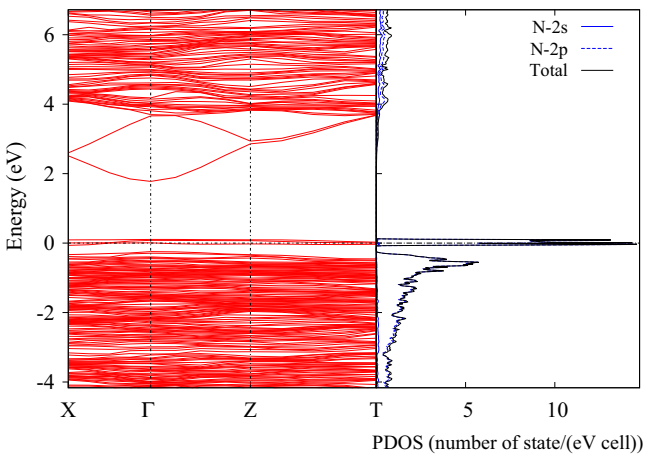

FIG. 4. Band structure and PDOS on the nearest neighbor atoms for V_{Ge} in $q = 0$ state. In this and subsequent band structure plots, the zero of energy is the Fermi energy.

$ZnGeN_2$, each N is surrounded by two Zn and two Ge atoms. Nominally, the Zn atoms share 1/2 electron per dangling bond with 3/2 electrons from N in a Zn-N bond, while the Ge atoms share each one electron per bond with one from N in the Ge-N bond. Thus around a V_{Ge} we have four N dangling bonds with four electrons in the neutral charge state. In a tetrahedral environment, the dangling bonds form an a_1 linear combination, which usually lies below the VBM and a triply degenerate t_2 state in the gap. Thus the t_2 state in this case has two electrons and room for up to four more in the $q = -4$ charge state. Thus the three bands we see in the band picture correspond to the t_2 state. It is not perfectly degenerate because of the lower than tetrahedral site symmetry as mentioned earlier. As we populate these bands with electrons, the level shifts deeper into the gap and eventually for the $q = -4$ state, even the lower a_1 symmetry band emerges out of the VBM.

The three defect levels in the gap have indeed quite localized defect wave functions. They are shown in Fig. 5. In Ref. [32], we provide additional data files which allow to view this and similar figures in 3D, rotate the models, zoom in, etc. We label the states as lowest unoccupied molecular orbital (LUMO), highest occupied molecular orbital (HOMO), and so on. Note that in the $q = -2$ state, the LUMO becomes HOMO and the LUMO+1 becomes LUMO and in the $q = -4$ state, the LUMO+1 becomes HOMO. This is clearly a deep acceptor.

Moving on to the V_{Zn}, we have a similar situation but now in the neutral charge state, the N-dangling bonds are already filled with four electrons. So, it can maximally occur in a $q = -2$ charge state. Its band structure and PDOS (Fig. 6) show again a sharp peak just above the VBM. It lies closer to the VBM than in the V_{Ge} case, indicating a shallower defect. In Fig. 7, we show the defect wave functions $|\psi_D|^2$ for the lowest unoccupied molecular orbital (LUMO), and the next two levels below it, HOMO, HOMO-1 for the $q = 0$ state. We can see that the LUMO is mostly localized in the plane of the vacancy and spreads out over first and second nearest nitrogen neighbors of the V_{Zn} in the a direction. The HOMO and HOMO-1 are more localized and spread in the b and c direction, respectively. All these states are reasonably well localized, although less than for the V_{Ge}. In particular, the LUMO state which becomes occupied with electrons in the $q = -1$ and $q = -2$ states is rather spread out. This state could be labeled a shallow acceptor. Both the V_{Ge} and V_{Zn} are clearly acceptors and therefore their wave functions are mostly localized on N atoms of the VBM.

2. Nitrogen vacancy

The V_N (Fig. 8) shows one defect level about 0.3 eV below the gap with the Fermi level passing through it in the neutral charge state. In creating a V_N, we remove eight valence states but only five electrons per vacancy. Thus the defect levels should accommodate three electrons. We can also think of these as residing in the Ge and Zn dangling bonds, which, respectively, provide one electron and half electron each. The defect level in the gap contains clearly just one electron, so there must be two more electrons in a defect state below it. On closer inspection one indeed can see a sharp peak in PDOS just above or at the VBM. So, that must be the other defect state. We can view the lower state as the a_1 combination

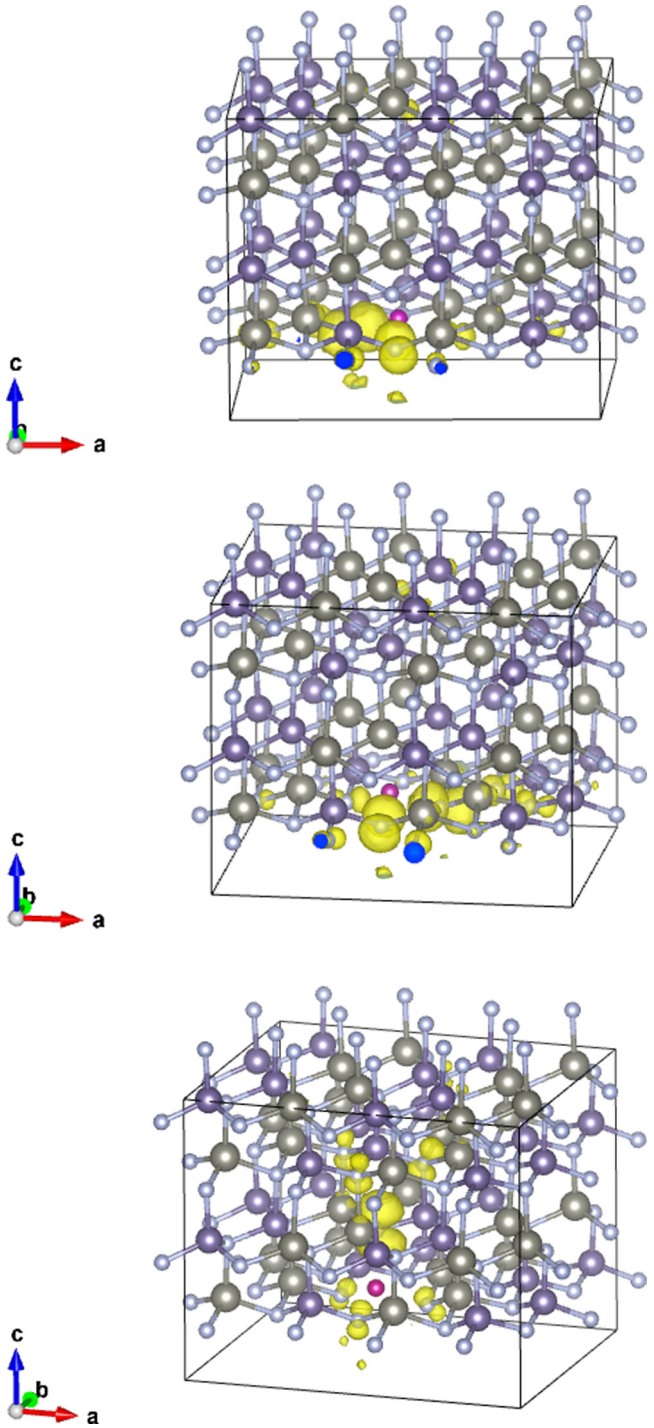

FIG. 5. Defect wave functions $|\psi_D|^2$, for V_{Ge} in $q = 0$ state, from top to bottom LUMO+1, LUMO, HOMO. The magenta sphere indicates the V_{Ge} site. In this and subsequent defect wave-function plots, the small grey spheres are N, the large grey spheres are Zn, and the large purple spheres are Ge. The figure shows a unit cell containing one defect. However, the calculated structure is periodic, so the charge densities shown as yellow isosurface should be viewed as periodically repeating. Thus some parts of this charge density near the edge of the cell may be closer to the defect in the neighboring cell.

of dangling bonds in a tetrahedral model, but inspecting this defect level wave function, it is found to be rather delocalized

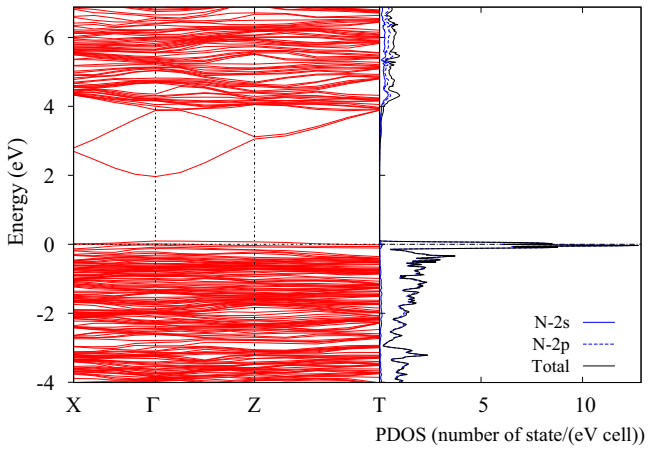

FIG. 6. Band structure and projected density of states on atoms near the V_{Zn} in $q = 0$ state.

and spread mostly over N atoms as can be seen in Fig. 9 for the HOMO-1 state. The level below the CBM (HOMO in the $q = 0$ state) on the other hand is very strongly localized on the two neighboring Ge atoms, consistent with the fact, that these atoms move inward toward the vacancy. We can also discern two additional bands above the CBM, which form resonances in the conduction band. Together with the defect level, these could be viewed as being derived from the t_2 tetrahedral linear combinations of Ge and Zn dangling bonds. In principle, this defect can support $q = +3, +2, +1, 0, -1$ states. Furthermore, the $q = 0$ and $q = 2$ states would have an unpaired spin ($S = 1/2$) and need to be studied including spin-polarization. The $+2$ and $+3$ states are expected to only occur if the Fermi level is very close the VBM. The defect can, in principle, both capture an electron or release an electron, so it could be viewed as a deep amphoteric trap level. However, we will show later that the negative charge state lies above the CBM, so it behaves rather like a deep donor.

Because the main defect level has a rather localized wave function it is not so clear how it will change when corrections of the gap beyond LDA are included. Therefore we need to closely examine how this level behaves with the LSDA+U method. In Fig. 10, we show the band structure and PDOS for the V_N^0 within the LSDA+U model described in Sec. II. We can see that the gap is now close to 3.4 eV, and the defect level for the majority spin lies a little deeper (0.5 eV) below the CBM than before. We now treated the system spin-polarized to take into account its net spin $S = 1/2$. In fact, the minority spin state of the defect level is seen to lie just below the CBM. We can still see two even sharper resonances in the conduction band and the lower one of these is now right at the CBM. Thus the character of the defect did not change by using LSDA+U. This is consistent with its defect character being very localized on Ge-s and Ge-p states. In the single positive charge state, the Fermi level becomes pinned at the lower defect level (the a_1 like level) and these states did not move at all because they are mostly N-p like and in that case, there is also no net magnetic moment.

3. *Antisite defects*

Next, we examine the antisite defects. For the Zn_{Ge} case, we show the band structure and PDOS in Fig. 11. We see

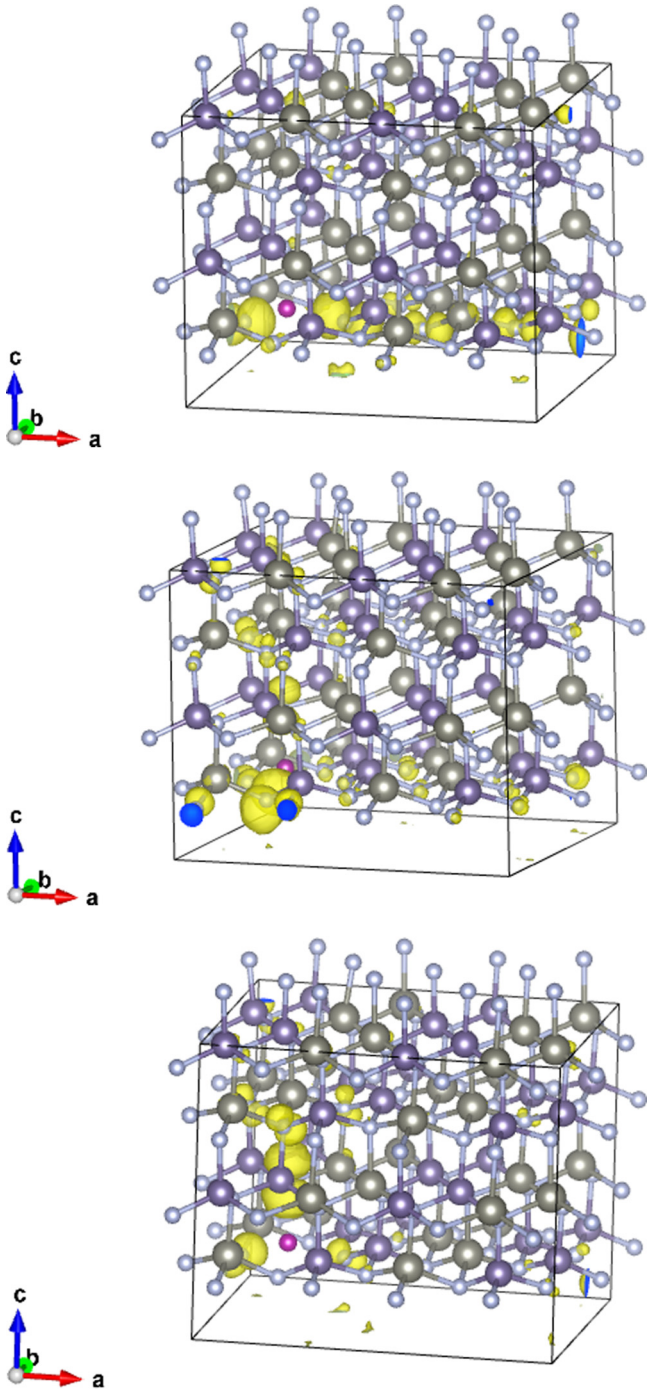

FIG. 7. Defect wave functions $|\psi_D|^2$, for V_{Zn} in $q = 0$ state, from top to bottom LUMO, HOMO, and HOMO-1. The magenta sphere indicates the V_{Zn} site.

a situation very similar to the V_{Zn}. This is indeed expected to be a double acceptor. It can take two extra electrons in a defect level just above the VBM in the band picture. Its LUMO wavefunction in the $q = 0$ state is shown in Fig. 12 and is seen to be fairly localized.

For Ge_{Zn} (Fig. 13), we find that in the neutral and even in the $q = +1$ charge state, the Fermi level lies well inside the conduction band. No states are seen in the gap. No changes in bands are discernible but for $q = +2$ the Fermi level shifts

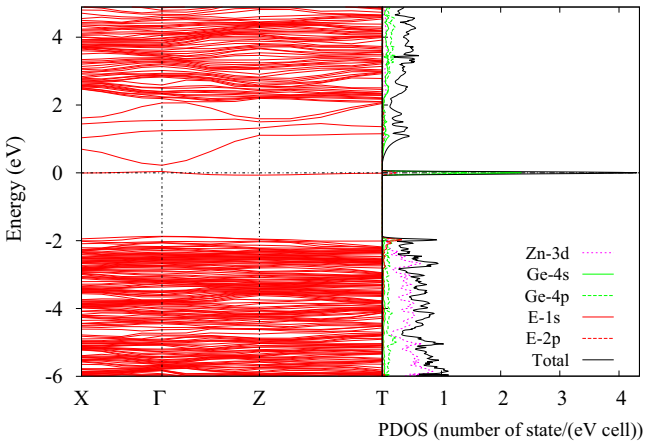

FIG. 8. Band structure and projected density of states on atoms near the V_N in $q = 0$ state.

to the VBM. This is a signature of a shallow donor state. One can see a resonance state in the CBM but not states in the gap. This is because a truly shallow donor state is spread well beyond the size of our supercell. Our model does not include the hydrogenic Coulomb tail $q/\varepsilon r$ that would extract a shallow

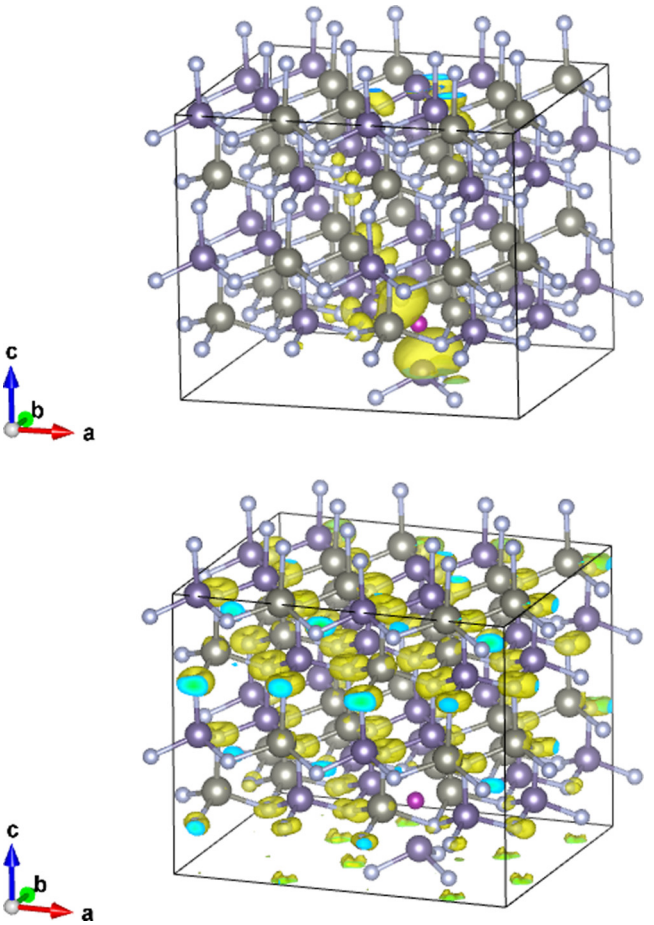

FIG. 9. Defect wave functions $|\psi_D|^2$, for V_N in $q = 0$ state, from top to bottom HOMO, HOMO-1. The magenta sphere indicates the V_N site.

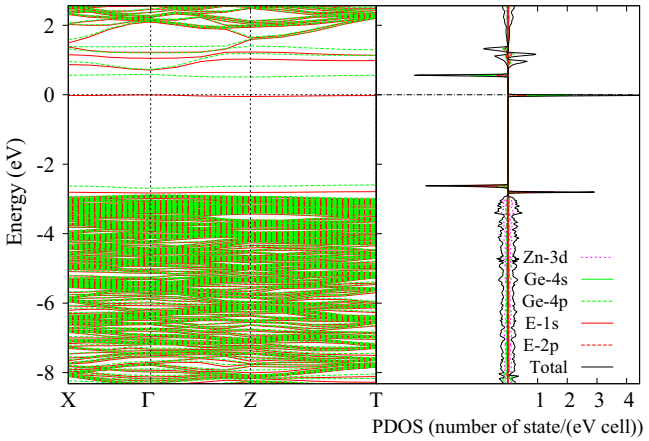

FIG. 10. Band structure and projected density of states on atoms near the V_N in $q = 0$ state using the LSDA+U method.

bound state below the CBM. Thus the Ge_{Zn} is a shallow double donor. We find that if we apply the LSDA+U method, still no state occurs in the gap. In other words, the resonance does not drop out of the CBM by shifting up the CBM. Thus we conclude that the shallow donor character of this defect is robust against gap corrections beyond LDA.

4. Impurities

We now examine various impurities. For oxygen, we performed calculations for O_{Ge}, O_{Zn} and O_N. For the cation locations of the O, we found strong relaxations including of the defect atom itself. We find that the O moves close to one of the surrounding N atoms and forms essentially an NO bond with bond lengths of about 1.2–1.3 Å. Two defect levels occur in the middle of the gap with several more close to the VBM. These are a mixture of O-p and dangling bonds on N or possibly a NO molecular state. In the Ge case, they contain two less electrons than in the Zn case in the neutral state. Both these defects, however, have much higher energies of formation of order 4–7 eV than for the N site and therefore we have not analyzed these situations in more detail and we do not show their band structure and PDOS results here because they are very unlikely to occur. They are, however, included in Ref. [32].

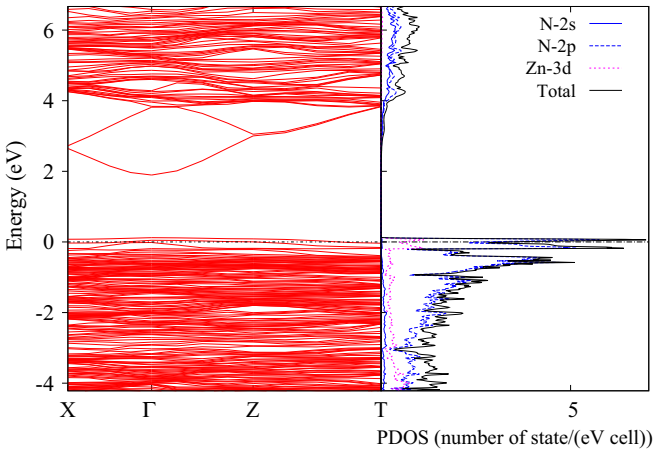

FIG. 11. Band structure and projected density of states on nearest atoms to the Zn_{Ge} antisite in the $q = 0$ state.

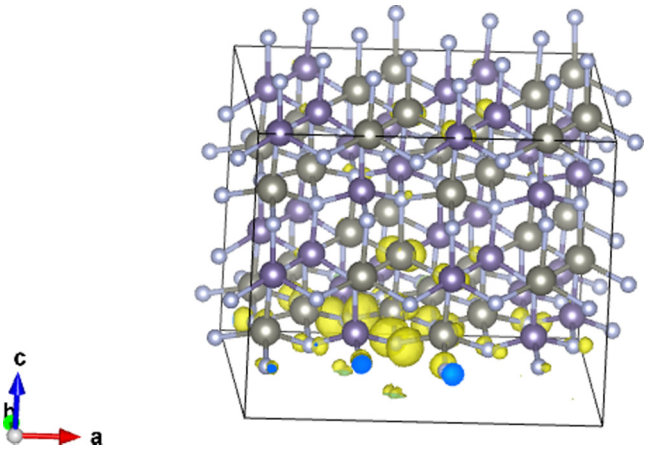

FIG. 12. Defect wave function $|\psi_D|^2$ for the LUMO in the Zn_{Ge} antisite in $q = 0$.

For the neutral charge state of O_N, the Fermi level lies within the conduction band. No defect states occur in the gap. In Fig. 14, we show the bands and PDOS for the $q = +1$ state when the Fermi level lies at the VBM. So, this is a shallow donor situation similar to Ge_{Zn}. We see again a resonant level slightly above the CBM. When using LSDA+U, we find a similar band structure. In other words, the resonance does not drop into the gap.

For Ga impurities, we need to consider both the Zn and Ge site. In the Ga_{Zn} case, we find a shallow donor situation similar to that of Ge_{Zn} except that it is a single donor. For Ga_{Ge}, we find a situation similar to that of Zn_{Ge} but now with single acceptor character. A peak corresponding to the acceptor defect level is seen in the band structure very close to or at the VBM. Band structure and PDOS figures are included in Ref. [32] for these cases.

C. Energies of formation

The energies of formation were calculated according to Eq. (1) using effective charges as explained in Sec. II E. For the shallow donors (Ge_{Zn}, O_N, and Ga_{Zn}), we place the formation energy of the defect in the state with the donor level occupied, at the bottom of the conduction band neglecting the

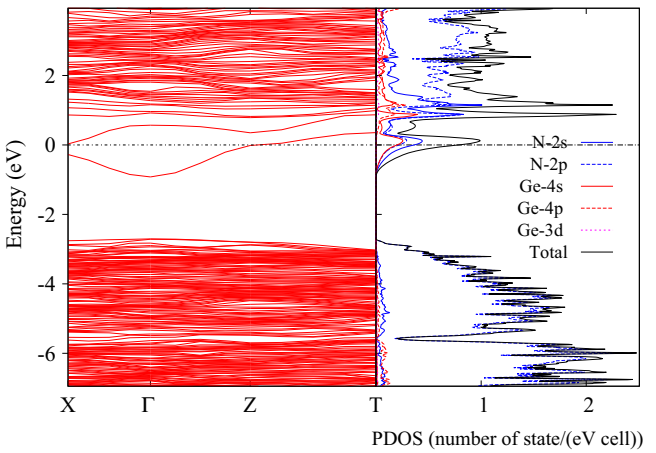

FIG. 13. Band structure and projected density of states on nearest atoms to the Ge_{Zn} antisite in the $q = +1$ state.

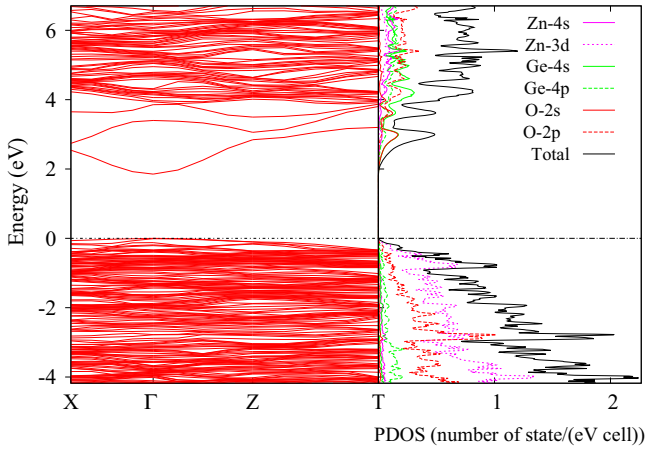

FIG. 14. Band structure and projected density of states on nearest atoms for O_N in $q = +1$ state.

small binding energy of the shallow donor. Likewise, for the shallow acceptor Ga_{Ge}, we calculate the neutral charge state assuming the $0/-$ transition level occurs close the VBM. This is equivalent to taking into account an effective point charge correction even for the neutral charge state. For the V_N, we found the $+2$ and $+3$ states to occur below the VBM, so they are not shown. We also include the LSDA+U shifts for the donors by shifting the $+/0$ transition of the V_N by the same amount as the one-electron level shifts in the band calculations. A similar correction shifts the $0/-$ state above the CBM. The acceptor transition levels are not affected by the gap correction and all lie somewhat deeper than the donors, at a few 0.1 eV above the VBM.

For Zn_{Ge}^{-1}, we find the electrostatic potential near the defect to look very similar to that for $q = 0$ and both are very flat. This can be related to the nature of the LUMO defect wave function in Fig. 11. While it is fairly localized on the Zn_{Ge} site itself and its nearest neighbor N atoms, there is also a tail in this distribution spread almost to the edge of the cell, at least in some directions. Thus the holes are in part compensating the nuclear charge deficit of Zn but in part also spread out. When we switch to the $q = -1$ state, we replace this delocalized hole charge by a background charge of the same sign, so nothing much changes. That is why the q_{eff} for this case is quite small. We estimate it as $q_{eff} = 0.3$.

The deeper acceptor levels are consistent with a hydrogenic model because of the much higher valence-band effective mass. We can make a simple estimate using the hydrogenic model. Averaging the inverse effective masses in the three directions, the top valence band gives an effective mass of 0.5 and this gives a binding energy of 70 meV for a single acceptor, 140 meV for a double acceptor and about 0.3 eV for a quadruple acceptor. These are probably underestimates because of the need for a central cell correction and the degeneracy of the VBM. For the donor states, only one charge state occurs as lowest energy in the gap, the $+1$ state for Ga_{Zn}, and O_N and the $+2$ charge state for Ge_{Zn}. Their $+/0$ or $2+/+$ transition levels are expected to occur within a few tens of meV below the CBM in a hydrogenic model but in our calculation we place it at the CBM itself. These donor levels were all found to follow the CBM when the gap is corrected using the LSDA+U method.

TABLE II. Formation energy (in eV) for various defects in different charge states at $\epsilon_F = 0$.

			$E_{for}(\epsilon_F = 0)$			
Defect	q	q_{eff}	A	B	C	D
V_{Ge}	0	0	9.52	8.82	9.09	10.21
	−1	−0.7	9.94	9.24	9.51	10.63
	−2	−1.5	11.75	11.05	11.32	12.44
	−3	−2	13.49	12.79	13.07	14.19
V_{Zn}	0	0	5.37	5.02	4.74	5.30
	−1	−0.5	5.53	5.18	4.90	5.46
	−2	−1.5	7.14	6.79	6.52	7.08
V_N	0	0	4.53	5.05	5.05	4.21
	1	1	1.94	2.47	2.47	1.63
Zn_{Ge}	0	0	2.61	2.26	2.82	3.38
	−1	−0.3	2.69	2.34	2.89	3.45
	−2	−1	4.09	3.74	4.29	4.85
Ge_{Zn}	2	1	− 0.73	− 0.38	− 0.94	− 1.50
O_N	1	1	− 3.30	− 2.78	− 2.78	− 3.62
O_{Ge}	0	0	7.03	6.33	6.61	7.73
	−1	−1	8.96	8.26	8.54	9.66
	−2	−2	11.87	11.17	11.45	12.57
O_{Zn}	0	0	6.03	5.68	5.41	5.97
	1	1	4.58	4.23	3.96	4.52
	−1	−1	6.69	6.34	6.07	6.63
	−2	−2	9.20	8.85	8.57	9.13
Ga_{Zn}	1	0.7	− 1.69	− 2.04	− 2.32	− 1.76
Ga_{Ge}	−1	−0.5	0.59	− 0.11	0.17	1.29

In Figs. 15 and 16, we allow the Fermi level ϵ_F to vary from the VBM at 0 energy to the actual experimental conduction-band minimum of 3.4 eV. In these figures we show only the energy of formation of the charge state with lowest energy at any given Fermi level position. The discontinuities in slope then indicate the transition levels. The figures show these energies for four different choices of chemical potential, as labeled in Fig. 1. Figure 15 corresponds to the native defects and Fig. 16 to the impurities. The energies of formation at $\epsilon_F = 0$ for various charge states which are used in drawing this figure are summarized in Table II. The transition levels are independent of chemical potentials and are summarized in Table III.

We note that the effective charges were determined by visual inspection of the fit of the electrostatic potentials by

TABLE III. Transition levels of various defects in $ZnGeN_2$.

Defect	Transition levels		
	+1/0	0/−1	−1/−2
V_{Zn}		0.16	1.62
V_N	2.58		
Zn_{Ge}		0.07	1.40
O_{Ge}		1.94	2.91
	0/−1		−1/−3
V_{Ge}	0.42		1.78
	+1/−1		−1/−2
O_{Zn}	1.06		2.50

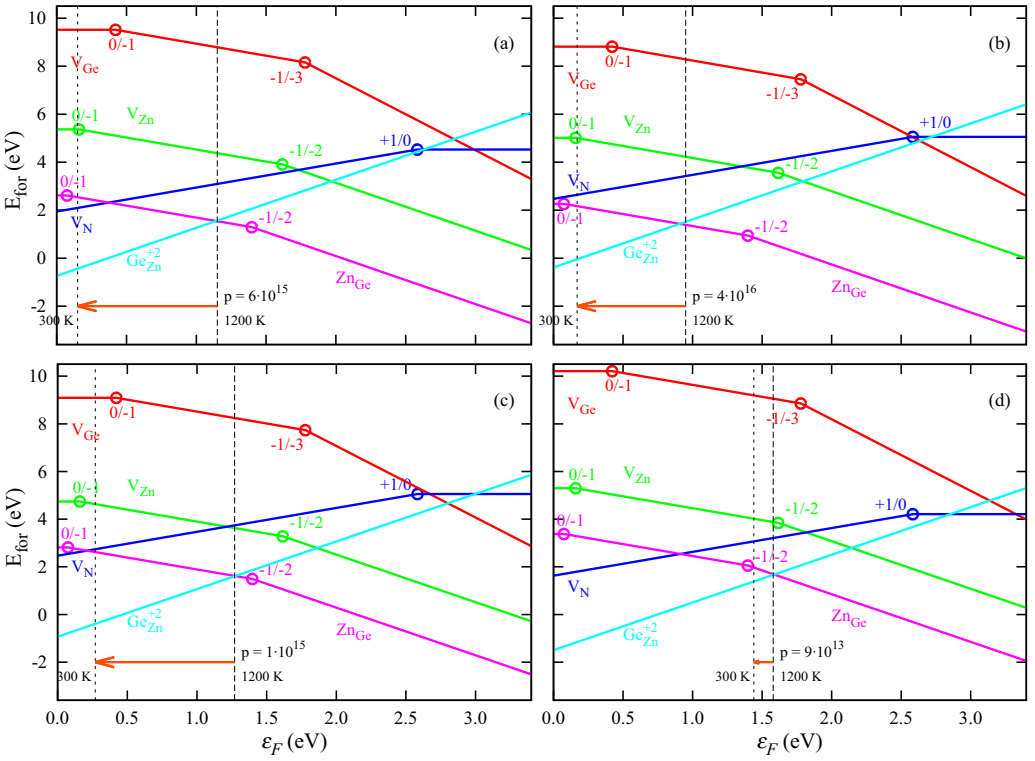

FIG. 15. Formation energies for different growing conditions (points A, B, C, and D on the diagram Fig. 1) for native defects V_{Ge}, V_{Zn}, V_N, Zn_{Ge}, and Ge_{Zn}.

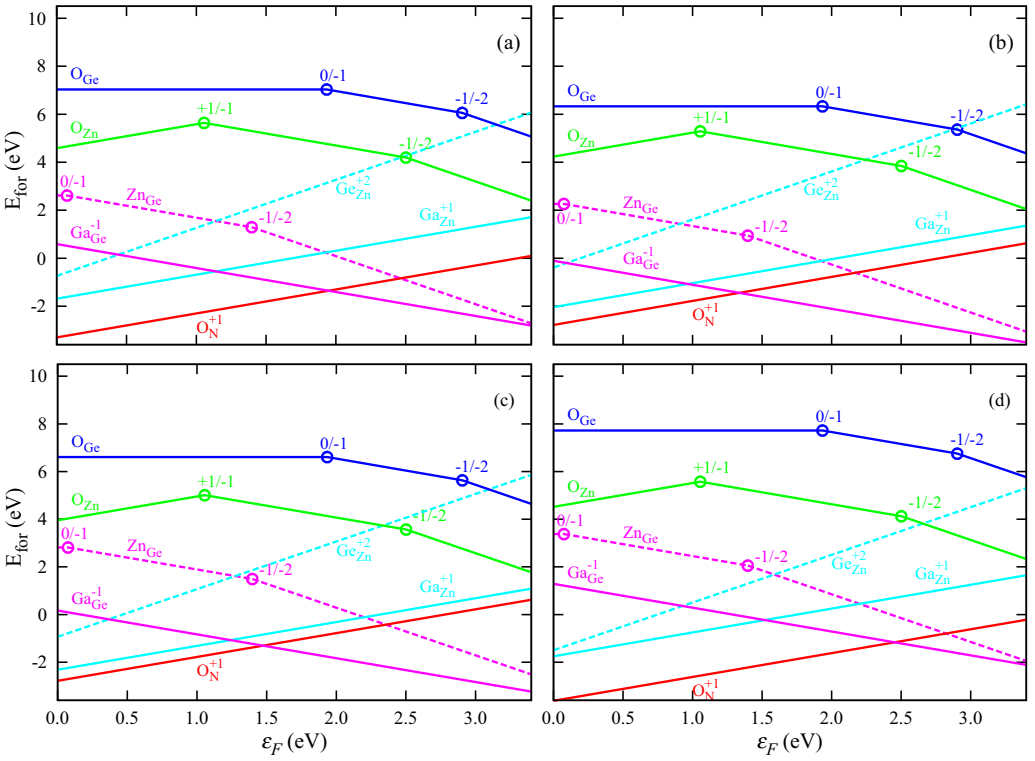

FIG. 16. Formation energies for different growing conditions (points A, B, C, and D on the diagram Fig. 1) for O_{Ge}, O_{Zn}, O_N, Ga_{Zn}, and Ga_{Ge} along with the two most important (lowest energy) native defects Ge_{Zn}, Zn_{Ge}.

a point charge model beyond a certain range. However, the precise value depends somewhat on the range chosen where the fit should apply. Thus these values and correspondingly the energies of formation and transition levels have an uncertainty of at least 0.1 eV. For example, for Zn_{Ge}, using the nominal charge we would have found the acceptor level at 0.48 eV, significantly deeper. The latter is most likely an overestimate, while the values obtained with $q_{\text{eff}} = 0.3$ may be a slight underestimate.

The $+/0$ level of V_N appears to be deeper below the CBM than the band structure plots indicated. However, this is because in the dilute limit the one-electron levels also need a finite size correction to the Madelung potential [24]. This would shift the levels by

$$\delta V = -\alpha q/(L\varepsilon). \tag{4}$$

This correction shifts acceptor levels up and donor levels down. For example, for V_N, we found the one-electron band in our 128 atom supercell about 0.5 eV below the CBM, adding this correction, it shifts down by about 0.36 eV and is then in good agreement with the $+/0$ transition level which lies 0.84 eV below the CBM. Thus the one-electron levels and transition levels are in good agreement with each other as required by the generalized Koopman's theorem. This also applies to the V_{Ge} acceptor levels, which are fairly deep. For the V_{Zn} and Zn_{Ge}, on the other hand, the correction is small because these are shallow acceptors.

Among the native defects, we see that the cation antisites have significantly lower energy than the vacancies. A similar conclusion was obtained for $ZnSnN_2$ by Chen *et al.* [33] and also for $ZnSnP_2$ by Kumagai *et al.* [16] but not for $ZnGeP_2$ [14,34–36]. We thus expect the dominant native defects to be the cation antisites.

In particular, the V_{Ge} is found to have a very high energy of formation even for the most Ge-poor conditions B and C. For example, for chemical potential condition A, we find that the energy of formation of the V_{Ge} 9.52 eV, is larger than the sum of the energies of formation of V_{Zn} and Zn_{Ge} which is 7.98 eV. This indicates an intrinsic thermodynamic instability or at least only metastability of the V_{Ge}. The neighboring Zn could hop to the V_{Ge} site forming a defect complex and then the two defects would repel each other. A similar situation was found for $ZnGeP_2$ [14]. We have not checked yet if there exists a barrier toward this defect reaction. Although this defect has high energy of formation in equilibrium, vacancies are easily created by radiation damage and may still be important.

Among the impurities, we see that O has indeed a definite site preference for the N position and the O_N is a very low-energy defect. This is similar to O_N in GaN [37]. Ga has a low energy of formation on the Zn site for Fermi levels close the VBM but Ga on the Ge site has a low energy of formation for Fermi levels close to the conduction band. The energies of formation of the Ga impurity are smaller than the corresponding antisite native defects. This is to be expected because they constitute a smaller perturbation. This indicates a good solubility of Ga is to be expected but with a site competition between both sites. Because this defect from the band structures appears to be a truly shallow hydrogenic type defect, our calculations do not predict the neutral charge state, in which the Fermi level lies below the VBM, well. Thus we use the approach for hydrogenic defect levels, or perturbed host states, as they are sometimes called and determine its neutral charge state formation energy assuming an acceptor level at the VBM.

D. Defect concentrations, Fermi level pinning, and doping

Assuming no other native defects are present, we can self-consistently determine the defect concentrations and Fermi level for a given set of chemical potentials. The defect concentrations are given by

$$C[D^q,\mu,T] = N[D^q]e^{-E_{\text{for}}(D^q,\mu)/kT}. \tag{5}$$

Here, $N[D^q]$ is the number of available sites per unit volume for a given defect times a degeneracy factor depending on the charge state. For example, if the defect has a singly occupied defect level, in which it can occur in two spin states, its degeneracy factor is 2 but if it is full occupied or empty, its degeneracy factor is 1. The energy of formation depends on the chemical potential of the electrons μ. $C[D^q,\mu,T]$ is the equilibrium concentration of defect D in charge state q and is a function of the Fermi level μ and temperature. The Fermi level is determined by the overall charge neutrality requirement:

$$-n(\mu,T) + p(\mu,T) + \sum_i q_i C\left[D_i^q,\mu,T\right] = 0. \tag{6}$$

Here, $n(\mu,T)$ is the concentration of electrons in the conduction band and $p(\mu,T)$ is the concentration of holes in the valence band, which are given by

$$\begin{aligned} n(\mu,T) &= \int_{\epsilon_c}^{\infty} D(\epsilon)f(\epsilon,\mu,T)d\epsilon, \\ p(\mu,T) &= \int_{-\infty}^{\epsilon_v} D(\epsilon)[1-f(\epsilon,\mu,T)]d\epsilon \end{aligned} \tag{7}$$

with

$$f(\epsilon,\mu,T) = \frac{1}{e^{\frac{\epsilon-\mu}{kT}}+1} \tag{8}$$

the Fermi function. Since realistically only the bottom of the conduction band and the top of the valence band contain electrons or holes, respectively, we calculate the electron and hole concentrations assuming a parabolic approximation to the band dispersions, which leads to

$$\begin{aligned} n(\mu,T) &= -2\left(\frac{m_n kT}{\pi\hbar^2}\right)^{3/2} \text{Li}_{3/2}\left(-e^{(\mu-\epsilon_c)/kT}\right) \\ &\approx 2\left(\frac{m_n kT}{\pi\hbar^2}\right)^{3/2} e^{-(\epsilon_c-\mu)/kT}, \\ p(\mu,T) &= -2\left(\frac{m_p kT}{\pi\hbar^2}\right)^{3/2} \text{Li}_{3/2}\left(-e^{(\mu-\epsilon_v)/kT}\right) \\ &\approx 2\left(\frac{m_p kT}{\pi\hbar^2}\right)^{3/2} e^{-(\mu-\epsilon_v)/kT}, \end{aligned} \tag{9}$$

where $Li_{3/2}(x)$ is the Polylogarithm (also known as the Jonquière) function, and ϵ_c is the one-electron energy of the CBM. The approximate forms with a Boltzmann type factor are valid when $\epsilon_c - \mu \gg kT$ and $\mu - \epsilon_v \gg kT$ and hold except very close to the band edges. The effective masses m_n and m_p here are so-called density of states masses. For $ZnGeN_2$,

TABLE IV. Equilibrium electron chemical potential (in eV), electron and hole concentrations, and defect concentrations, all per cm^3. The values at 300 K assume the total defect concentration is quenched from 1200 K. Open slots in the table correspond to negligible concentrations less than 10^5.

	A		B		C		D	
T(K) →	1200	300	1200	300	1200	300	1200	300
μ (eV)	1.15	0.15	0.95	0.17	1.27	0.27	1.58	1.44
n	6.0×10^9		8.2×10^8		1.9×10^{10}		3.8×10^{11}	
p	6.0×10^{15}	5.3×10^{15}	4.4×10^{16}	4.3×10^{16}	1.9×10^{15}	8.0×10^{14}	9.6×10^{13}	
Ge_{Zn}^{+2}	5.5×10^{15}	5.5×10^{15}	9.8×10^{15}	9.8×10^{15}	3.7×10^{15}	3.7×10^{15}	2.1×10^{15}	2.1×10^{15}
Zn_{Ge}^{0}	2.3×10^{11}	2.2×10^{13}	6.8×10^{12}	6.9×10^{14}	3.3×10^{10}	1.7×10^{12}	1.5×10^{8}	
Zn_{Ge}^{-1}	1.6×10^{16}	1.6×10^{16}	6.3×10^{16}	6.3×10^{16}	7.1×10^{15}	8.2×10^{15}	6.3×10^{14}	7.2×10^{14}
Zn_{Ge}^{-2}	7.30×10^{14}		4.0×10^{14}		1.1×10^{15}		1.9×10^{15}	1.8×10^{15}
V_N^{+1}	4.3×10^9	4.3×10^9	2.0×10^8	2.0×10^8	8.4×10^6	8.4×10^6	1.4×10^9	1.4×10^9
V_{Zn}^{-1}					2.6×10^7	2.6×10^7	2.3×10^6	3.1×10^6

which has an orthorhombic crystal structures, as discussed in Punya *et al.* [1], $m_n^{3/2} = (m_a m_b m_c)^{3/2}$ with m_a, m_b, and m_c the effective conduction-band masses along the a, b, and c directions. The valence band in this material is split in three levels, and expressions of the above type are applied separately for each level with the appropriate effective masses given in Table VII of Ref. [1].

First, we only consider native defects. The concentrations of defects are evaluated at a typical growth temperature of 1200 K. Using the above analytical expressions, it is then straightforward to find the μ for which the charge neutrality is obeyed. From the energy of formations, it is easy to see that the Boltzmann factors will suppress all but the lowest energy of formation defects. This implies in this case that the Fermi level μ is essentially determined by the competition between the Ge_{Zn}^{2+} and Zn_{Ge}^{-1} defects and the free electrons and holes. We checked, that using only these two defects or all of the defects, made almost no difference in the resulting Fermi level, which for chemical potential condition B is 0.95 eV above the VBM, slightly above the crossing of the energies of formation of these two defects. Since this Fermi level position is closer to the VBM than to the CBM, the net resulting doping is p type with a concentration of holes $p \approx 4.4 \times 10^{16}$ cm^{-3} at 1200 K.

We also consider the electron and hole concentration at room temperature (300 K) assuming that the total concentration in all possible charge states stay the same as at 1200 K, but their charge state can adjust to a new neutrality condition at 300 K. In other words, the defect concentrations are quenched but the electrons and holes adjust to the Fermi function at 300K and so do the charge states of the defect according to their relative Boltzmann factors. This leads to a Fermi level position much closer to the VBM, $\mu = 0.17$ eV and a slightly lower hole concentration of $p \approx 4.3 \times 10^{16}$ cm^{-3}. Clearly, at lower temperature, in order to keep the same carrier concentration of holes to compensate the Zn_{Ge}^{-1}, the Fermi level will need to move closer to the VBM. Meanwhile, both the concentration of Ge_{Zn}^{2+} and of electrons in the conduction band are fairly low because for low Fermi energy, the energy of formation of Ge_{Zn}^{2+} is higher and so fewer of these defects are generated.

In Fig. 15, we indicate the equilibrium Fermi level at 1200 and at 300 K with their corresponding p-type hole concentration. In Table IV, we give the equilibrium concentrations of the different defects as well as the Fermi level position and net electron and hole concentrations at 1200 K and after quenching to 300 K for each of the chemical potential conditions A-D. We can see that our calculations predict the materials to be native p type with a significant hole concentration up to 10^{16} cm^{-3} if the chemical conditions are chosen optimally as in case B.

There have thus far been very few reports on the carrier type in $ZnGeN_2$. Larson *et al.* [38] reported their samples to be n type with a carrier concentration $n \approx 10^{18}$–10^{19} cm^{-3}, while Kikkawa and Morisaka [39] reported their samples to be insulating. The first group used a vapor growth method which involves $ZnCl_2$ and $GeCl_4$ as intermediate products. Cl is likely to be an n-type dopant if present in the samples. Kikkawa and Morisaka [39] used a sputter growth technique. Very recently, Dyck *et al.* [40] used Seebeck coefficient measurements and reported n-type behavior. The n-type behavior apparently cannot be explained by the native defects considered here. Although Ge_{Zn}^{2+} is a shallow donor and has fairly low energy of formation for $\epsilon_F = \epsilon_v$, the charge balance dictates a Fermi level closer to the VBM by competition with the Zn_{Ge}^{-1} acceptors. Being closer to the VBM, we then obtain more holes than electrons.

On the other hand, we see from Fig. 16 that substitutional O_N is a very low-energy defect and since it is a donor, it might lead to n-type doping. To be more precise about the incorporation of O, we need to consider the chemical potentials of O and N at finite temperature. In other words, we need to consider their free energies including entropic contributions. The most important contribution here is the pressure term

$$\mu_N = \mu_N(N_2) + kT \ln(p_{N_2}) \tag{10}$$

with a similar expression for oxygen. We ignore the smaller vibrational and rotation free energy terms since they are similar in both molecules. In the O_N energy of formation, we need $\mu_N - \mu_O$ so, what enters is the ratio p_{N_2}/p_{O_2}. In other words, the concentration of O_N is given by

$$C[O_N^+] = 2\left(\frac{p_{O_2}}{p_{N_2}}\right)\left(\frac{8}{V_{cell}}\right)e^{-(E_{for}(O_N,\mu=0)+\mu)/kT}. \tag{11}$$

We recalculate the Fermi level position and the corresponding defect concentrations and effective doping from the neutrality condition including the O_N^{+1} defect for various

ratios of the partial pressure ratios $p(N_2)/p(O_2)$ for the case of chemical potentials B. At low $p_{N_2}/p_{O_2} = 10$, we find a very large oxygen concentration, of order 10^{24} cm^{-3}, leading essentially to an oxynitride. However, there is then also a high concentration of Zn_{Ge} in both -1 and -2 charge states, compensating the positive charge, so we end up with a Fermi level near 2 eV and a low net n-type doping of 10^{13} cm^{-3}. In this sense, $ZnGeN_2$ differs strongly from GaN. In GaN, the only native acceptor is a V_{Ga}^{-3} and this defect has high energy and thus crosses the O_N^{+1} only very close to the VBM. In contrast, $ZnGeN_2$ has a low-energy antisite acceptor Zn_{Ge}.

At 300 K, keeping the defect concentrations fixed, the Fermi level drops to 1.58 eV, the electrons are less easily excited to the CBM and thus play even less a role in compensating the O_N^{+1} and we find insulating behavior. This means that oxygen should be strongly suppressed during growth to keep the concentration of both O_N^{+1} and Zn_{Ge}^{2-} down. At 1200 K, we need to increase the p_{N_2}/p_{O_2} ratio to about 10^6 to switch from n to p type. The p-type concentration is then of order only 10^{12} cm^{-3} at 1200 K but the concentration of Zn_{Ge} and O_N is still of order 10^{21}. Only for a partial pressure ratio as high as 10^{15}, the O_N and Zn_{Ge} at the growth temperature could be suppressed to the 10^{15} cm^{-3} level, to recover the native p-type concentration level of 10^{16} cm^{-3} at 300 K.

Thus the question arises if oxygen could still explain the unintentional n-type doping. If the sample is exposed to air after cooling down, oxygen could still enter the sample because it has a very low energy of formation. However, diffusion will be limited at these temperatures and thus, we can probably not assume equilibrium any more. Nonetheless, it appears plausible that the regions near the surface or in small particles of polycrystalline material, some oxygen uptake could take place even if it was avoided during growth. In this case, we no longer expect Zn_{Ge} antisites to be able to form and hence it would then lead to residual n-type doping. Another possible source for n-type dopants would be interstitials. We thus plan to study interstitials in a future study.

Finally, we examine the effects of Ga doping. The optimal condition for introducing Ga preferentially on the Ge rather than the Zn site is the Ge poorest situation B. We choose this condition as we are aiming for p-type doping. In that case, because the system is rich in N, we assume the $\mu_{Ga} = \mu_{Ga}^0 + E_{for}(GaN)$. We find the Fermi level now becomes pinned close to the intersection of the Ga_{Zn}^{+1} and Ga_{Ge}^{-1} energies of formation, with the Fermi energy at about 1.00 eV above the VBM. This leads to a p-type doping of order 2.5×10^{16} cm^{-3} at 1200 K. We find the concentrations $[Ga_{Zn}^{+1}] = 4.592 \times 10^{19}$ cm^{-3} and $[Ga_{Ge}^{-1}] = 4.583 \times 10^{19}$ cm^{-3}. We can see that there is compensation of these two defects to 1 part in a 100 with slightly more donors than acceptors. However, there also is a sizable concentration of Zn_{Ge}^{-1} of 1.1×10^{17}cm^{-3}, which help to tip the balance in favor of p-type behavior. The net hole type concentration however is actually slightly lower than we found earlier for the native material under growth condition B. If we now quench to 300 K, the Fermi level drops to 0.20 eV but the hole concentration drops only slightly to 1.2×10^{16} cm^{-3}. So, Ga acts indeed as a p-type dopant but is not more effective than the intrinsic doping by Zn_{Ge}, which assists it.

IV. CONCLUSIONS

In summary, we have presented a study of the main expected native defects and a few dopants in $ZnGeN_2$. The main findings of the paper are as follows. Cation antisites are the dominant native defects. The Ge_{Zn}^{+2} shallow donor and Zn_{Ge}^{-1} shallow acceptor states pin the Fermi level at a position closer to the VBM than the CBM and hence should lead to native p-type doping. The level of this doping depends on the chemical potential conditions and is also still somewhat uncertain due to the uncertainties in our calculation of the energies of formation related to finite size corrections. Upon quenching to room temperature, the Fermi level moves closer to the VBM but still could retain a fairly significant level of p-type doping level. The n-type doping one has found so far in $ZnGeN_2$ is tentatively ascribed to O_N. Although the latter has a low energy of formation, it would be compensated by formation of native antisite acceptors Zn_{Ge}^{2-} at the growth temperature. This is different from GaN where no low energy compensating acceptors exist. This actually predicts very little residual n-type doping at room temperature when defect concentrations are frozen. To explain residual background n-type doping by oxygen, we then need to assume that during the cooling down of the sample, more oxygen is introduced then compensating antisites formed. Alternatives such as interstitials need further study.

In terms of methodology, we discussed the various finite size effects and proposed to model the defect electrostatic potentials with a point charge model, which, however, could have a different effective charge from the nominal charge of the defect. This tends to reduce the energies of formation and the transition levels of the acceptor for relatively shallow acceptors. Unfortunately, the effective charge has still some remaining uncertainty. The latter could presumably be further reduced by using larger supercells.

ACKNOWLEDGMENTS

A.P. and L.-y.H. were supported by the National Science Foundation (NSF) under Grant No. DMR-1104595 in early stages of the work, D.S. was supported by the U.S. Department of Energy Basic Energy Sciences (DOE-BES) under Grant No. DE-SC0008933. W.L. was supported by both grants and in the final stages of the work by NSF under grant DMR-1533957. Calculations were performed at the Ohio Supercomputer Center under Project No. PDS0145.

[1] A. Punya, W. R. L. Lambrecht, and M. van Schilfgaarde, Phys. Rev. B **84**, 165204 (2011).

[2] T. J. Peshek, T. R. Paudel, K. Kash, and W. R. L. Lambrecht, Phys. Rev. B **77**, 235213 (2008).

[3] T. R. Paudel and W. R. L. Lambrecht, Phys. Rev. B **78**, 115204 (2008).
[4] T. R. Paudel and W. R. L. Lambrecht, Phys. Rev. B **79**, 245205 (2009).
[5] W. R. L. Lambrecht and A. Punya, in *III-Nitride Semiconductors and their Modern Devices*, edited by B. Gill (Oxford University Press, Oxford, UK, 2013), pp. 519–585.
[6] P. C. Quayle, E. W. Blanton, A. Punya, G. T. Junno, K. He, L. Han, H. Zhao, J. Shan, W. R. L. Lambrecht, and K. Kash, Phys. Rev. B **91**, 205207 (2015).
[7] N. Feldberg, J. D. Aldous, W. M. Linhart, L. J. Phillips, K. Durose, P. A. Stampe, R. J. Kennedy, D. O. Scanlon, G. Vardar, R. L. Field *et al.*, Appl. Phys. Lett. **103**, 042109 (2013).
[8] P. Hohenberg and W. Kohn, Phys. Rev. **136**, B864 (1964).
[9] W. Kohn and L. J. Sham, Phys. Rev. **140**, A1133 (1965).
[10] U. von Barth and L. Hedin, J. Phys. C **5**, 1629 (1972).
[11] http://www.lmsuite.org/.
[12] M. Methfessel, M. van Schilfgaarde, and R. A. Casali, in *Electronic Structure and Physical Properties of Solids. The Use of the LMTO Method*, edited by H. Dreyssé, Lecture Notes in Physics Vol. 535 (Berlin Springer Verlag, 2000), p. 114.
[13] T. Kotani and M. van Schilfgaarde, Phys. Rev. B **81**, 125117 (2010).
[14] X. Jiang, M. S. Miao, and W. R. L. Lambrecht, Phys. Rev. B **71**, 205212 (2005).
[15] F. Bruneval, J.-P. Crocombette, X. Gonze, B. Dorado, M. Torrent, and F. Jollet, Phys. Rev. B **89**, 045116 (2014).
[16] Y. Kumagai and F. Oba, Phys. Rev. B **89**, 195205 (2014).
[17] C. Freysoldt, J. Neugebauer, and C. G. Van de Walle, Phys. Rev. Lett. **102**, 016402 (2009).
[18] C. Freysoldt, J. Neugebauer, and C. G. Van de Walle, Phys. Status Solidi B **248**, 1067 (2011).
[19] C. Freysoldt, B. Grabowski, T. Hickel, J. Neugebauer, G. Kresse, A. Janotti, and C. G. Van de Walle, Rev. Mod. Phys. **86**, 253 (2014).
[20] F. Oba, A. Togo, I. Tanaka, J. Paier, and G. Kresse, Phys. Rev. B **77**, 245202 (2008).
[21] H.-P. Komsa, T. T. Rantala, and A. Pasquarello, Phys. Rev. B **86**, 045112 (2012).
[22] M. Leslie and N. J. Gillan, J. Phys. C **18**, 973 (1985).
[23] D. Segev and S.-H. Wei, Phys. Rev. Lett. **91**, 126406 (2003).
[24] Y. Kumagai, M. Choi, Y. Nose, and F. Oba, Phys. Rev. B **90**, 125202 (2014).
[25] G. Makov and M. C. Payne, Phys. Rev. B **51**, 4014 (1995).
[26] V. I. Anisimov, J. Zaanen, and O. K. Andersen, Phys. Rev. B **44**, 943 (1991).
[27] V. I. Anisimov, F. Aryasetiawan, and A. I. Lichtenstein, J. Phys. Condens. Matter **9**, 767 (1997).
[28] A. I. Liechtenstein, V. I. Anisimov, and J. Zaanen, Phys. Rev. B **52**, R5467 (1995).
[29] S. L. Dudarev, G. A. Botton, S. Y. Savrasov, C. J. Humphreys, and A. P. Sutton, Phys. Rev. B **57**, 1505 (1998).
[30] A. Boonchun and W. R. L. Lambrecht, Phys. Status Solidi B **248**, 1043 (2011).
[31] A. Boonchun and W. R. L. Lambrecht, Phys. Status Solidi B **250**, 2091 (2013).
[32] See Supplemental Material at http://link.aps.org/supplemental/10.1103/PhysRevB.93.155202 for a full set of band structure, partial density of states, and defect charge density.
[33] S. Chen, P. Narang, H. A. Atwater, and L.-W. Wang, Adv. Mater. **26**, 311 (2014).
[34] L. E. Halliburton, G. J. Edwards, M. P. Scripsick, M. H. Rakowsky, P. G. Schunemann, and T. M. Pollak, Appl. Phys. Lett. **66**, 2670 (1995).
[35] N. C. Giles, L. E. Halliburton, P. G. Schunemann, and T. M. Pollak, Appl. Phys. Lett. **66**, 1758 (1995).
[36] N. C. Giles, L. Bai, M. M. Chirila, N. Y. Garces, K. T. Stevens, P. G. Schunemann, S. D. Setzler, and T. M. Pollak, J. Appl. Phys. **93**, 8975 (2003).
[37] J. Neugebauer and C. G. Van de Waller, *Native Defects and Impurities in GaN* (Vieweg, Braunschweig/Wiesbaden, 1996), Vol. 35, pp. 25–43.
[38] W. L. Larson, H. P. Maruska, and D. A. Stevenson, J. Electrochem. Soc. **121**, 1673 (1974).
[39] S. Kikkawa and H. Morisaka, Solid State Commun. **112**, 513 (1999).
[40] J. S. Dyck, J. R. Colvin, P. C. Quayle, T. J. Peshek, and K. Kash, J. Electron. Mater. (2016), doi:10.1007/s11664-015-4322-3.